ADVANCED ENERGY MATERIALS
www.advenergymat.de

Optimization of the Output Efficiency of GaN Nanowire Piezoelectric Nanogenerators by Tuning the Free Carrier Concentration

*Chao-Hung Wang, Wei-Shun Liao, Zong-Hong Lin, Nai-Jen Ku, Yi-Chang Li, Yen-Chih Chen, Zhong-Lin Wang, and Chuan-Pu Liu**

As fossil fuels are consumed at an extremely fast rate, various types of renewable energy technologies have been developed to either replace or work with traditional energy power plants. Recently, piezoelectric nanogenerators (NGs) have been proposed for scavenging mechanical energy from movements or vibrations. Both direct-current (DC)[1,2] and alternating-current (AC)[3–5] NGs have been demonstrated. Piezoelectric NGs can be incorporated into devices to make them self-powered. Examples include self-powered systems for wireless communications[6] and self-driving liquid-crystal displays.[7] High-output-voltage NGs[8] have promise in practical biomechanical applications.

Piezoelectric NGs produce electricity via strain-induced piezoelectric potential (piezopotential), which is created by inner-crystal ionic polarization. Piezopotentials are induced by immobile piezoelectric charges accumulated at the two ends of a nanomaterial under deformation, and alter charge transport behavior at the interface between a piezoelectric semiconductor and a metal contact, which is referred to as the piezotronic effect. With this effect, traditional transistors can be simplified as two terminal piezotronic transistors that can be adopted for active and adaptive tactile imaging sensors.[9] Coupled to light, these piezoelectric charges have been utilized to enhance the conversion efficiency of light-emitting diodes[10] and solar cells[11] in addition to the sensitivity of photodetectors[12] and active imaging pressure sensors[13] via the piezo-phototronic effect. The piezotronic and piezo-phototronic effects expand the applications of piezoelectric semiconductor materials.

For developing high-output-power NGs, the geometrical design and inner resistance of semiconductor nanomaterials have been shown to be paramount, both in experiments[14,15] and calculations.[16–19] The room-temperature carrier concentration in semiconductors is often overlooked in the design of NGs, even though it is one of the most fundamental characteristics and can be easily tuned through doping and photoexcitation. For instance, it has been demonstrated that the output performance of n-type ZnO-based NGs can be enhanced by p-type doping,[20] but decreased with higher hole concentration achieved with antimony (Sb).[21] Surface passivation improves the output voltage of NGs under UV illumination because the carrier screening effect is minimized.[22] This implies that the doping concentration greatly affects NG performance and should thus be studied in depth. However, its effect has rarely been studied due to the lack of an efficient method of controlling the defect levels inside intrinsic ZnO.

GaN, which has a low intrinsic electron concentration and is insensitive to the ambient, is an ideal model material for the investigation of the carrier concentration effect on the output performance of NGs. In this work, a series of Si-doped GaN nanowire (NW) arrays was employed to study the carrier screening effect on piezopotential, and thus the output power of NGs.

The basic semiconductor and crystal properties of the GaN NW arrays synthesized by plasma-assisted molecular beam epitaxial (PA-MBE) system were investigated since they enormously influence the power generation and the mechanisms of electricity generation of NGs. The typical diameter and density of the as-grown vertically aligned n-GaN NW arrays are ≈50 nm and 7.95×10^{10} cm^{-2}, respectively, as shown in **Figure 1**a, while the length is ≈500 nm after 2 h growth. Figure 1b shows a typical high-resolution TEM (HR-TEM) image of a NW. The GaN NWs exhibit high crystallinity without noticeable linear or planar defects. Moreover, the spacing of the lattice fringes is measured to be ≈0.251 nm, which corresponds to the *c*-plane interplanar distance of a GaN crystal. The polarity of the GaN NWs was found to be *–c* polar with respect to the growth direction. A detailed crystal polarity characterization is presented in the Supporting Information.

C.-H. Wang, W.-S. Liao, Dr. N.-J. Ku, Y.-C. Li, Dr. Y.-C. Chen, Prof. C.-P. Liu
Department of Materials Science and Engineering
National Cheng Kung University
Tainan 70101, Taiwan
E-mail: cpliu@mail.ncku.edu.tw
Dr. Z.-H. Lin, Prof. Z.-L. Wang
School of Materials Science and Engineering
Georgia Institute of Technology
North Avenue, Atlanta, GA 30332, USA
Prof. C.-P. Liu
Department of Materials Science and Engineering
National Cheng Kung University
Tainan 70101, Taiwan
Prof. C.-P. Liu
Center for Micro/Nano Science and Technology
National Cheng Kung University
Tainan 70101, Taiwan
Prof. C.-P. Liu
Research Center for Energy Technology and Strategy
National Cheng Kung University
Tainan 70101, Taiwan

DOI: 10.1002/aenm.201400392

ADVANCED ENERGY MATERIALS
www.advenergymat.de

www.MaterialsViews.com

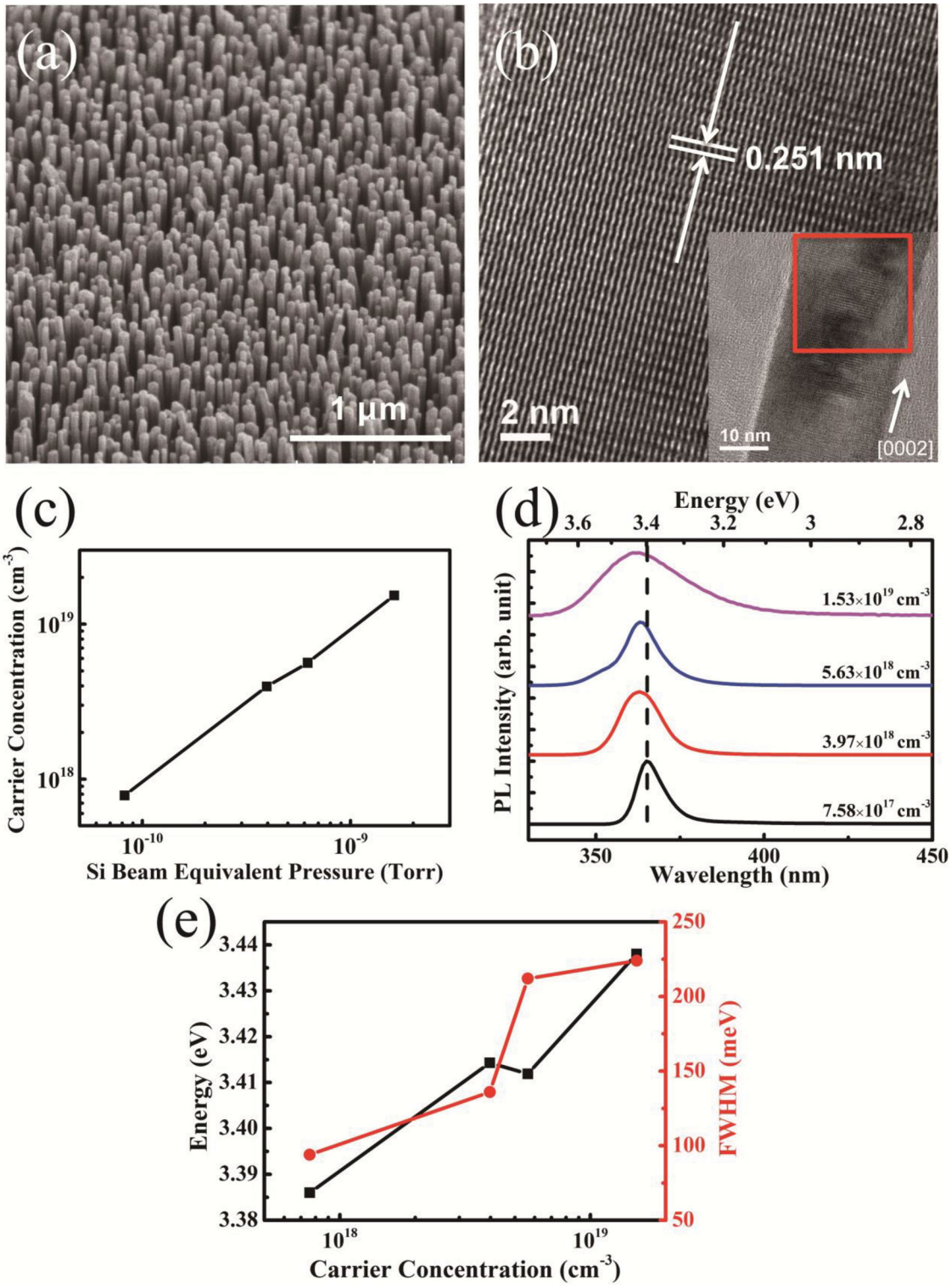

Figure 1. MBE-grown GaN NW arrays. a) Tilted SEM image and b) HR-TEM image of a single GaN NW taken from the red rectangular region of the lower magnification image in the inset. c) Raman-determined carrier concentration versus Si BEP. d) PL spectra of n-GaN NW arrays with four different carrier concentrations and e) PL peak energy and FWHM values versus carrier concentration of n-GaN NW arrays.

For Si-doped GaN NW arrays, the carrier concentration increases with doping concentration, as determined from Raman spectra through the phonon-plasmon coupled mode of a GaN Raman peak.[23] The determined carrier concentrations are listed as a function of Si beam equivalent pressure (BEP) in the Supporting Information. Figure 1c shows that with varying

Si BEP, the carrier concentration linearly changes in the range of 7.58×10^{17} to 1.53×10^{19} cm^{-3} for this series. The carrier concentration significantly affects luminescence behavior, as revealed by the photoluminescence (PL) spectra in Figure 1d, where the near-band-edge emission shifts toward higher energy and broadens gradually with increasing carrier concentration. Specifically, the peak position shifts from 3.385 to 3.435 eV and the full width at half maximum (FWHM) increases from 100 to 225 meV, as demonstrated in Figure 1e, which can be attributed to the well-known Burstein-Moss (B-M) effect of doping. These results confirm that Si doped into GaN NWs increases electron concentration.

For semiconductor materials, both carrier type and carrier concentration are of paramount importance. Carrier concentration induces physical phenomena such as the screening effect, which is the dominant driver for reducing piezopotential inside piezoelectric semiconductor materials, which are the building blocks of NGs. In order to investigate the effect of carrier screening on NG performance, the device architecture, substrate effect, and NG core (piezoelectric nanomaterial) are discussed in the following.

Regarding the device architecture, n-GaN NW arrays with a doping concentration of 7.58×10^{17} cm^{-3} were assembled into vertically integrated nanogenerator (VING) devices using polymethyl methacrylate (PMMA) to fill the gaps between NWs to increase mechanical robustness and prevent electrical shortening, as illustrated in **Figure 2**a. In this design, when the device is subjected to cyclic pressing and releasing at 2 Hz with a maximum force of about 5 kgf (corresponding to approximately 1 MPa), the resulting peak output voltage and current density in the AC output pulses are typically ≈80 mV and 10 nA cm^{-2}, respectively, as demonstrated in Figure 2b,c. An examination of the output voltage and current pulses indicates that the peak value on the positive pulses is always slightly higher than that on the negative pulses. For voltage pulses, this may be ascribed to the difference in strain rate between the straining and restoring induced by the PMMA layer. The current inconsistency between pulses is caused by charge loss. To further explore this issue, typical complete cycles in Figure 2b,c are enlarged in **Figure 3**a,c, respectively, where the current density is integrated with time to follow the evolution of the total charge density during electricity generation. A voltage pulse cycle can be divided into four regions corresponding to response/recovery under either pressing or releasing. The characteristic times of these stages are denoted as $T_{\text{Resp-Press}}$, $T_{\text{Recov-Press}}$, $T_{\text{Resp-Release}}$, and $T_{\text{Recov-Release}}$, respectively. For clarity in interpretation, those characteristic times labeled in Figure 3a are extracted and demonstrated in Figure 3b. Figure 3b shows that the overall response and recovery under pressing is longer than that upon releasing. This means that the time for power generation during releasing is shorter than that during straining, giving rise to the higher voltage peak during releasing to satisfy energy conservation. With in-depth investigation, we consider the response time when the force constraint is applied and diminished, according to $T_{\text{Resp-Press}}$ and $T_{\text{Resp-Release}}$. These response times are correlated to the device structure, with the PMMA layer affecting the conduction of the external force to the GaN NWs. Because of the lower Young's modulus of PMMA compared to GaN,[19] the straining in GaN NW arrays is not coherent in

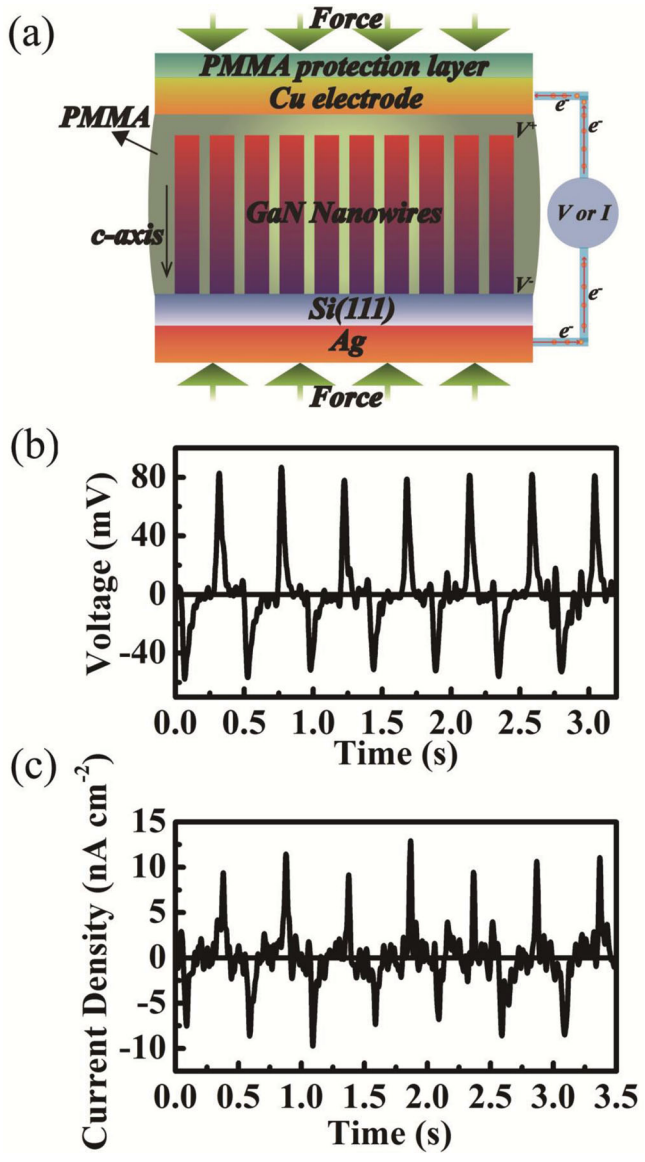

Figure 2. a) VING device structure and electrical circuit schematic of a VING containing GaN NW arrays. b) Output voltage and c) current density of a VING prototype versus time.

response to the external force during compression, producing a slightly lower straining rate compared to the compression rate. When the external force is diminished, the strain in the GaN NW arrays quickly responds. The different strain rates result in inconsistency in the peak between positive and negative cycles. The recovery time is the time needed for passivating the piezopotential during pressing and that needed for returning the piezopotential back to equilibrium state during releasing, which is determined by the transport of electrons through the interface across the device. As illustrated in Figure S2 (Supporting Information), when the piezopotential is established under pressing, electrons move from the GaN NWs, Si substrate, and Ag electrode, powering the external load to the Cu electrode and passing through two interfaces, namely GaN/Si and Si/Ag. Based on this principle, the recovery process takes more time

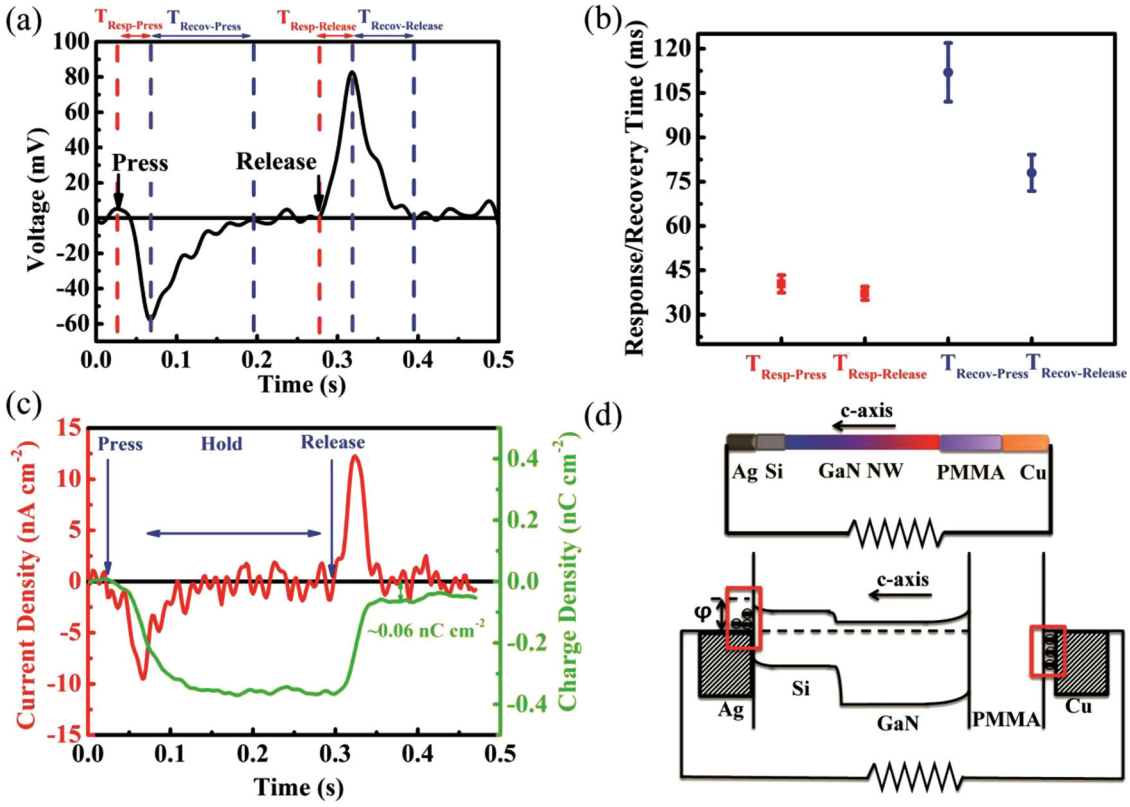

Figure 3. a) One cycle of output voltage of a VING divided into four steps ($T_{Resp\text{-}Press}$, $T_{Recov\text{-}Press}$, $T_{Resp\text{-}Release}$, and $T_{Recov\text{-}Release}$). b) Four characteristic times extracted from (a). c) Current density and charge density (integrated current density) over three stages of electricity generation. d) Device structure and energy band diagram of the final stage of power generation, showing that some electrons are left behind.

during pressing than it does during releasing because electrons pass through more interfaces. It is noteworthy that the polymer used here focused exclusively on mechanical-electrical interaction of the VING rather than its dielectric constant. It has been reported that the lower the dielectric constant of the polymer, the worse the VING performs.[19] Therefore, PMMA was utilized for all devices for experimental consistency.

Current loss may occur in this cyclic process, as shown in Figure 3c. When a compressive normal force is applied to the VING, based on the polarity of the GaN NWs, a positive piezopotential is established at the interface to PMMA and a negative piezopotential is established to Si substrate. Electrons are forced to flow from the VINGs through the Ag electrode to the Cu electrode via an external circuit to balance the piezopotential, as shown in Figure S2a (Supporting Information). The charges accumulate up to ≈0.40 nC cm^{-2}. When the piezopotential is fully screened after a short period of time, no more currents flow and thus there is no output current. This steady state is referred to as the "Hold" state, as shown in Figure 3c. When the normal force is released, the steady state no longer holds because the piezopotential is diminished. The electrons thus flow back from the Cu electrode to the Ag electrode into the device, as shown in Figure S2c (Supporting Information), but some electrons are blocked by the Schottky barrier at the Ag/Si interface, as shown in Figure 3d. This barrier leads to charge loss of ≈0.06 nC cm^{-2} during the electricity generation process, reducing the efficiency of VINGs.

After the basic mechanism of a single VING had been examined, the effect of carrier concentration on VINGs was investigated. Previous simulation results[19] showed that carrier concentration greatly affects the output characteristics of piezoelectric NGs. However, this effect has rarely been investigated experimentally. Here, GaN NW arrays doped with Si were used for exploring this issue since their carrier concentration can be varied systematically. Carrier concentration is expected to greatly influence the output characteristics of a piezoelectric NG because it alters the inner resistance of piezoelectric semiconductor materials, especially for DC NGs. In an AC NG, carrier concentration should also strongly affect the remnant piezopotential inside the piezoelectric semiconductor material via the screening effect of excess carriers. However, the dependence of carrier concentration on the degradation of the output performance of an NG is still unclear. A series of VING devices made of GaN NW arrays with various carrier concentrations, ranging from 7.58×10^{17} to 1.53×10^{19} cm^{-3}, were tested. Their output performances are shown in **Figure 4**. The average peak output voltage of the VING dropped from ≈70 mV for the lightly doped device gradually down to ≈4 mV for the heaviest doped device, as shown in Figure 4a,b. The output current density follows the same decreasing trend. The average maximum output charge density, normalized to the current density for a fair comparison, decreases from ≈0.464 to ≈0.064 nC cm^{-2}, as shown in Figure 4c,d. The results show that when the carrier concentration is increased by about 20-fold, the output voltage

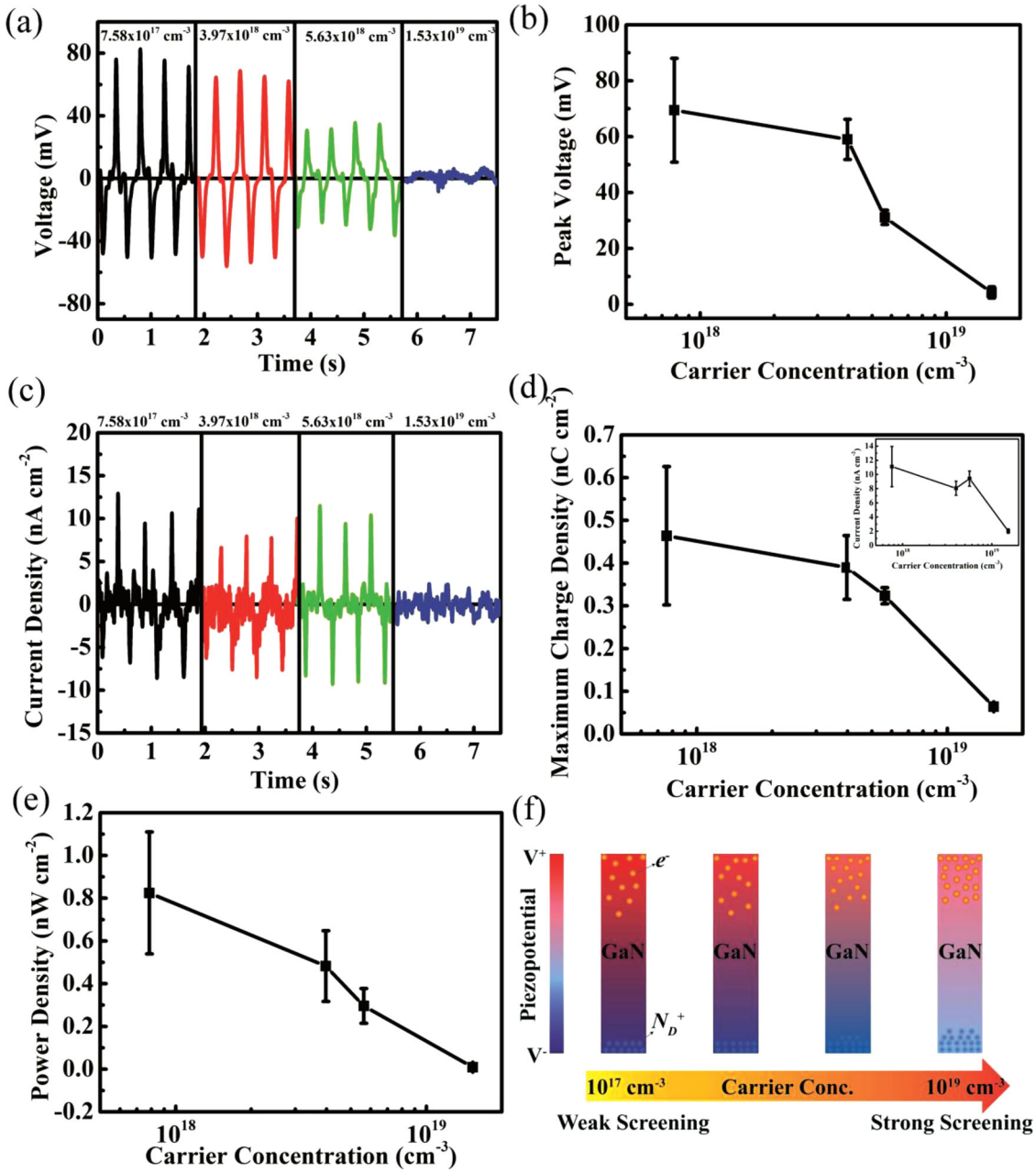

Figure 4. a) Output voltage and b) extracted average output voltage of four VINGs with n-GaN NW arrays with different carrier concentrations. c) Current density and d) maximum charge density versus carrier concentration. The inset of (d) shows current density versus carrier concentration. e) Power density of VINGs for various carrier concentrations. f) Schematic of illustrating screening effect on piezopotential under various carrier concentrations. The electrons (e^-) tend to screen the positive piezopotential, while the ionized donors (N_D^+) compensate the negative piezopotential. The higher the carrier concentration, the smaller the output piezopotential.

decreases by about 17.5-fold. There is therefore a linear relationship between the carrier concentration and average output voltage. This provides strong evidence that the carrier screening effect on the piezopotential is responsible for the reduced output voltage, assuming that the piezoelectric coefficient of n-GaN remains almost the same as pure GaN because of only a small fraction of parent lattices being subsituted for dopants. The free carriers degrade the piezopotential output by about 17.5-fold, with the minimum output piezopotential almost diminished. Although it has been shown that the remnant piezopotential in ZnO nanomaterials is nearly fully screened by free carriers at high concentrations of over $\approx 10^{18}$ cm^{-3},[19] our experiments reveal that an order higher free carrier concentration is needed to fully eliminate the piezopotential inside GaN NWs. This discrepancy may be ascribed to the different fundamental material properties between GaN and ZnO, such as electron screening length, activation energy of the dopant, electron density of states, etc. The maximum output power density can be calculated as:

$$P_{max} = J_{sc-max} \times V_{oc-max} \quad (1)$$

where $J_{sc\text{-}max}$ and $V_{oc\text{-}max}$ are the maximum short-circuit current density and open-circuit voltage, respectively. The calculation results are shown in Figure 4e. There is a monotonic decrease from ≈0.8 to ≈0 nW cm^{-2} with increasing carrier concentration. According to the results, a higher power output is obtained with a lower carrier concentration, but a lower power output is gained at a high carrier concentration of 1.53×10^{19} cm^{-3} simply due to the strongly screened piezopotential. For AC NGs, the carrier concentration greatly affects the output characteristics. The carrier screening effect on the output piezopotential is further illustrated by a schematic in Figure 4f where the electrons and ionized donors tend to compensate the positive and negative piezopotentials, respectively, causing the remaining output piezopotential reduced. As a result, the more the carriers are, the stronger the screening effect is, leading to diminishing output voltage. The lowest possible carrier concentration is favorable for producing the highest output power becuase the screening effect is inhibited. This outcome is different from that for DC NGs, which require an optimal carrier concentration for generating the maximum electrical power.

In conclusion, AC VING devices composed of n-GaN NW arrays grown on Si with various doping concentrations were packaged with PMMA polymer as a dielectric and mechanical strengthening layer. The PMMA layer provides a robust structure but its dielectric constant is suboptimal, especially for force conduction, which results in different strain rates during pressing and releasing. The Si substrate epitaxially matches the GaN NW arrays and provides good electrical conductivity, but leads to some charge loss due to the energy barrier created by the energy band mismatch between the metal electrode and the substrate. The GaN NW arrays, the core of the VING devices, produce piezopotential in response to an applied force. The screening effect greatly affects the output performance of VINGs. In the design of high-power VING devices, controlling or even inhibiting the screening effect is of importance for enhancing the output performance.

In summary, Si-doped GaN NW arrays grown via MBE with a precisely controlled Si doping concentration were fabricated. The emission peak of Si-doped GaN NW arrays shifts towards higher energy with increasing doping concentration because of the B-M effect. The positive and negative voltages generated by the VING devices are not equal owing to the resistance of force conduction by the surrounding layer of PMMA and the presence of an energy barrier between the metal electrode and Si substrate, which causes charge loss. GaN NW arrays are strongly influenced by the carrier concentration. The screening effect greatly affects the output characteristics of VINGs. The output voltage dropped by 17.5-fold when the carrier concentration was increased by about 20-fold, implying that the carrier screening effect is the dominant driver responsible for deteriorating the piezopotential. In addition, the maximum power density monotonically decreases with increasing carrier concentration. The lower the carrier concentration is, the higher the power output of AC NGs that can be harvested.

Experimental Section

Vertically aligned GaN NW arrays were grown without any catalysts on n-type Si(111) substrates using an ultrahigh-vacuum, radio-frequency, plasma-assisted molecular beam epitaxial (PA-MBE) system (SVTA 35-Nitride MBE) under a nitrogen-rich environment and a high substrate temperature. Except for the doping concentration, all the GaN NW arrays were grown using the same growth conditions, with the nitrogen-to-Ga flux ratio, plasma power, substrate temperature, and growth time fixed at 40, 350 W, and 760 °C, and 2 h, respectively. Silicon was utilized as the n-type dopant. The electron concentration was systematically tuned by varying the beam equivalent pressure (BEP) controlled by the silicon effusion cell temperature. The morphology of the as-grown n-GaN NWs was investigated by scanning electron microscopy (SEM, Hitachi SU-8000) and their crystal structure was examined using transmission electron microscopy (TEM, JEOL JEM-2100F). Micro Raman (μ-Raman) spectroscopy and PL spectroscopy (HORIBA Jobin Yvon/Labram HR) were employed to determine the doping concentration and optical emission properties of the Si-doped GaN NWs. Finally, AC GaN piezoelectric NGs were fabricated in the form of VINGs, as shown in Figure 2a, where 100-nm-thick polymethyl methacrylate (PMMA) was infused to completely encapsulate the NW arrays as an electron-blocking layer instead of forming a metal-semiconductor Schottky barrier with a metal electrode. The output voltage and current of the NGs were measured using low-noise voltage and current preamplifiers (SR560 and SR570, respectively, Standford Research Systems).

Supporting Information

Supporting Information is available from the Wiley Online Library or from the author.

Acknowledgements

This work was financially supported by the National Science Council (NSC) of Taiwan under grants NSC 101–2221-E-006–131-MY3, NSC 101–2622-E-006–015-CC1, and NSC 101–2622-E-006–005-CC1. The authors would like to thank the Instrument Center of National Cheng Kung University, and the NSC Core Facilities Laboratory for Nano-Science and Nano-Technology in the Kaohsiung-Pingtung area for providing equipment and technical support.

Received: March 5, 2014
Revised: May 14, 2014
Published online: June 27, 2014

[1] X. Wang, J. Song, J. Liu, Z. L. Wang, *Science* **2007**, *316*, 102.
[2] J. Liu, P. Fei, J. Song, X. Wang, C. Lao, R. Tummala, Z. L. Wang, *Nano Lett.* **2007**, *8*, 328.
[3] R. Yang, Y. Qin, L. Dai, Z. L. Wang, *Nat. Nanotechnol.* **2009**, *4*, 34.
[4] S. Xu, Y. Qin, C. Xu, Y. Wei, R. Yang, Z. L. Wang, *Nat. Nanotechnol.* **2010**, *5*, 366.
[5] G. Zhu, R. Yang, S. Wang, Z. L. Wang, *Nano Lett.* **2010**, *10*, 3151.
[6] Y. Hu, Y. Zhang, C. Xu, L. Lin, R. L. Snyder, Z. L. Wang, *Nano Lett.* **2011**, *11*, 2572.
[7] Y. Hu, Y. Zhang, C. Xu, G. Zhu, Z. L. Wang, *Nano Lett.* **2010**, *10*, 5025.
[8] G. Zhu, A. C. Wang, Y. Liu, Y. Zhou, Z. L. Wang, *Nano Lett.* **2012**, *12*, 3086.
[9] W. Wu, X. Wen, Z. L. Wang, *Science* **2013**, *340*, 952.
[10] Q. Yang, W. Wang, S. Xu, Z. L. Wang, *Nano Lett.* **2011**, *11*, 4012.
[11] X. Wen, W. Wu, Z. L. Wang, *Nano Energy* **2013**, *2*, 1093.

[12] Q. Yang, X. Guo, W. Wang, Y. Zhang, S. Xu, D. H. Lien, Z. L. Wang, *ACS Nano* **2010**, *4*, 6285.
[13] C. Pan, L. Dong, G. Zhu, S. Niu, R. Yu, Q. Yang, Y. Liu, Z. L. Wang, *Nat. Photonics* **2013**, *7*, 752.
[14] N. J. Ku, C. H. Wang, J. H. Huang, H. C. Fang, P. C. Huang, C. P. Liu, *Adv. Mater.* **2013**, *25*, 861.
[15] R. Araneo, G. Lovat, P. Burghignoli, C. Falconi, *Adv. Mater.* **2012**, *24*, 4719.
[16] Y. Gao, Z. L. Wang, *Nano Lett.* **2009**, *9*, 1103.
[17] G. Mantini, Y. Gao, A. D'Amico, C. Falconi, Z. Wang, *Nano Res.* **2009**, *2*, 624.
[18] G. Romano, G. Mantini, A. Di Carlo, A. D'Amico, C. Falconi, Z. L. Wang, *Nanotechnology* **2011**, *22*, 465401.
[19] R. Hinchet, S. Lee, G. Ardila, L. Montès, M. Mouis, Z. L. Wang, *Adv. Funct. Mater.* **2014**, *24*, 971.
[20] J. I. Sohn, S. N. Cha, B. G. Song, S. Lee, S. M. Kim, J. Ku, H. J. Kim, Y. J. Park, B. L. Choi, Z. L. Wang, J. M. Kim, K. Kim, *Energy Environ. Sci.* **2013**, *6*, 97.
[21] K. C. Pradel, W. Wu, Y. Zhou, X. Wen, Y. Ding, Z. L. Wang, *Nano Lett.* **2013**, *13*, 2647.
[22] T. T. Pham, K. Y. Lee, J. H. Lee, K. H. Kim, K. S. Shin, M. K. Gupta, B. Kumar, S. W. Kim, *Energy Environ. Sci.* **2013**, *6*, 841.
[23] K. Jeganathan, R. K. Debnath, R. Meijers, T. Stoica, R. Calarco, D. Grützmacher, H. Lüth, *J. Appl. Phys.* **2009**, *105*, 123707.

